Nanoscale

Accepted Manuscript

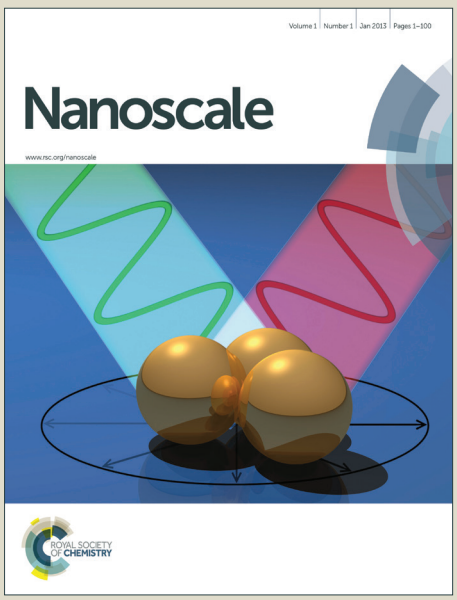

ROYAL SOCIETY OF CHEMISTRY

www.rsc.org/nanoscale

Journal Name

ARTICLE

3D graphene oxide microchip and Au-enwrapped silica nanocomposite-based supersandwich cytosensor toward capture and analysis of circulating tumor cells

Received 00th January 20xx,
Accepted 00th January 20xx

DOI: 10.1039/x0xx00000x

www.rsc.org/

Na Li[a,b], Tingyu Xiao[a,b], Zhengtao Zhang[a], Rongxiang He[a,b], Dan Wen[a], Yiping Cao[a,b,†], Weiying Zhang[a,b,†] and Yong Chen[a,b,c]

Determination of the presence and number of circulating tumor cells (CTCs) in peripheral blood can provide clinically important data for prognosis and therapeutic response patterns. In this study, a versatile supersandwich cytosensor was successfully developed for the highly sensitive and selective analysis of CTCs using Au-enwrapped silica nanocomposites (Si/AuNPs) and three-dimensional (3D) microchips. First, 3D microchips were fabricated with a photolithography method. Then, the prepared substrate was applied to bind graphene oxide, streptavidin and biotinylated epithelial-cell adhesion-molecule antibody, resulting in high stability, bioactivity, and capability for CTC capture. Futhermore, horseradish peroxidase and anti-CA153 were co-linked to the Si/AuNPs for signal amplification. The performance of the cytosensor was evaluated with MCF7 breast cancer cells. Under optimal conditions, the proposed supersandwich cytosensor showed high sensitivity with a wide range of 10^1 to 10^7 cells mL^{-1} and a detection limit of 10 cells mL^{-1}. More importantly, it could effectively distinguish CTCs from normal cells, which indicated the promising applications of our method for the clinical diagnosis and therapeutic monitoring of cancers.

Introduction

Cancer is considered a worldwide mortal sickness and has become a major public concern. Metastasis is the most common cause of cancer-related deaths in patients with solid tumors. During the progression of metastasis, tumor cells detach from the solid primary tumor, enter the blood stream and travel to different tissues of the body.[1] These "break-away" tumor cells in the peripheral blood are known as circulating tumor cells (CTCs). In addition to conventional diagnostic imaging and serum marker detection, CTC analysis as a "liquid biopsy" can provide valuable information on prognosis, facilitate monitoring of systemic anticancer therapy, and help to identify appropriate therapeutic targets.[2] However, as the concentration of CTCs is generally extremely low (a few to hundreds per milliliter) in the bloodstream, detection and characterization of CTCs presents a tremendous technical challenge.[3, 4] Over the past decade, various technology platforms for isolating/counting CTCs have been developed using different strategies such as flow cytometry, immune magnetic beads, mechanical separation, or microfluidic devices.[5-8] However, the sensitivity of these emerging technologies relies on the degree of enrichment of CTCs. Thus, the development of a novel and sensitive platform that enhances CTC capture, allows for imaging of the captured CTCs, and enables quantitative analysis would dramatically increase the use of CTCs in diagnostics and prognostics.

Graphene and its derivatives have attracted considerable attention due to their extremely large surface area, biocompatibility, excellent electrocatalytic activity, fast electron transfer, strong mechanical strength and high chemical stability.[9] Owing to these extraordinary properties, graphene and its nanocomposites have been widely applied to modify a glassy carbon electrode (GCE) for immobilizing various biomolecules.[10-14] Thus, most of the graphene based electrochemical sensors developed to date show two designs: the assembly of two-dimensional (2D) graphene on the GCE or multi-stacked graphene films. Further integration of the widely available graphene sheets as 2D-nanoscale building blocks into a functional three-dimensional (3D) system is essential to extend their biomedical applications.[15] Recently, a 3D hierarchical nanostructured graphene oxide (GO) platform combined with a ZnO nanorod array was successfully utilized to recognize/capture ethithelial cell-adhesion molecule (EpCAM)-expressing cancer cells.[16] The mechanism relies on the enhanced local topographic interactions between the substrate and nanoscale components of the cellular surface, which improve the capture efficiency of target cells to a certain extent.[17-22]

Herein, we present a convenient and cost-efficient 3D microchip coated with GO and EpCAM antibody (anti-EpCAM, Ab1)

[a] Flexible Display Mater. & Tech. Co-Innovation Center of Hubei, Institute for Interdisciplinary Research, Jianghan University, Wuhan 430056, PR China
[b] Key Laboratory of Optoelectronic Chemical Materials and Devices of Ministry of Education, Jiang Han University, Wuhan 430056, PR China
[c] Ecole Normale Supérieure, CNRS-ENS-UPMC UMR 8640, 24 Rue Lhomond, Paris 75005, France
† Corresponding Author: zwy2428@163.com; cyp@jhun.edu.cn

to serve as a cytosensor for the capture and analysis of CTCs. With the remarkable development of nanotechnology, nanomaterials have been extensively used to enhance the sensitivity of cytosensors. Among them, gold nanoparticles (AuNPs) are of particular interest owing to their merits of high surface reactivity, good solubility, unique optical and electronic characteristics as well as their excellent biocompatibility.[23-25] Thus, clever combinations of different types of functional nanostructured materials will enable the development of multifunctional nanomedical platforms for diagnosis and therapy. Among various integrated nanocomposite-based systems, mesoporous silica-based nanostructured materials have attracted great interest, since they exhibit low cytotoxicity and excellent chemical stability, and their surface can be easily modified.[26-29] Therefore, they are ideal platforms for constructing multifunctional materials that incorporate a variety of functional nanostructured materials.

In this study, we developed a novel CTC-sensitive quantitative detection system that integrates two functional components: (1) a 3D microchip with GO and anti-EpCAM coating for recognizing/ capturing EpCAM-expressing cells, and (2) Au-enwrapped silica nanocomposites (Si/AuNPs) loaded with horseradish peroxidase (HPR) and anti-CA153 (Ab2) to improve the selectivity of target cells and amplify the electrochemical detection signal. The 3D microchip arrays were initially prepared as illustrated in Scheme 1A. The microchips were subsequently modified by GO, streptavidin (SA), and biotinylated anti-EpCAM, respectively, which served as 3D bioelectronics interfaces (Scheme 1B). In addition, the Si/AuNPs were synthesized (Scheme 1C), and then used as matrices to load the high-density signaling enzymes HPR and Ab2. As a proof-of-concept, MCF7 breast cancer cells were selected as model cells because of their high levels of EpCAM and CA153 expression to demonstrate the feasibility of the supersandwich strategy. Finally, when sandwich-type immunoreactions were carried out (Scheme 1D), the HRP on the surface could catalyze the oxidation of H_2O_2 in the presence of thionine, which served as an electron transfer mediator. The proposed strategy exhibited excellent sensitivity and selectivity, indicating its wide applicability for research and clinical evaluations of cancer progression.

Experimental

Materials and reagents

The polydimethylsiloxane (PDMS) prepolymer kit was purchased from Momentive Performance Materials (Waterford, NY). Positive photoresist AZ 40XT-11D and the developer AZ-300MIF were obtained from AZ Electronic Materials Corp. (Philadelphia, PA). DMEM medium for cell culture was obtained from GIBCO. 1-(3-(Dimethylamino)-propyl)-3-ethylcarbodiimide hydrochloride (EDC), N-hydroxysulfosuccinimide (NHS), HPR, fluorescein diacetate (FDA) and SA were purchased from Sigma (St. Louis, MO). Biotinylated goat IgG polyclonal anti-EpCAM antibody and mouse monoclonal anti-CA153 antibody were obtained from R&D Systems (Minneapolis, MN). GO was obtained from Graphene Laboratories Inc. (Calverton, NY). All other chemicals used in this study were analytical-grade. All solutions were freshly prepared using ultrapure water (≥18 MΩ, Millipore).

Fabrication and surface modification of the 3D Microchip Device

All the 3D microchip devices were designed with L-Edit software and fabricated using a lithography fabrication technique, which is illustrated in Scheme 1. The device was approximately 1 × 1 cm. All of the microchip masters were fabricated by spin-coating with positive photoresist (AZ 40XT-11D) on a silicon substrate. Briefly, Step 1 (Scheme 1A a to c): a layer of AZ 40XT-11D was thrown at a clean and dry silicon wafer, which was then exposed to ultraviolet light through a high-resolution transparency mask (25,000 dpi). Step 2 (Scheme 1A d): a PDMS prepolymer mixture (oligomer: curing agent mass ratio = 10:1) was poured over the negative grooves, which were placed in suitable Petri dishes. Step 3 (Scheme 1A e): after curing at 80 °C for 2 h and peeling off the PDMS, positive linear arrays of 3D PDMS-based microchips were obtained. Scheme 1A (f) shows the scanning electron microscopy (SEM) images (Hitachi, S-3400N) of the prepared 3D microchip arrays.

A total of 100 mg of GO was dispersed in 200 mL ethanol (with 0.05 % chitosan) with ultrasonication for 30 min, and then 1 mL of the GO solution was mixed with 400 mM EDC and 100 mM NHS in 1 mL of MES buffer (pH 5.2) for 30 min at room temperature to activate the carboxyl groups on the surfaces of GO. After washing the mixture with phosphate-buffered saline (PBS), SA (50 μg/mL in PBS) was added to the solution at 4 °C for 2 h and subsequently washed three times with PBS to remove unreacted SA. Biotinylated anti-EpCAM (10 μg/mL in PBS) was finally added. The microchips were incubated with the resulting solution for 1 h at room temperature and dried to fabricate a functional film.

Synthesis of Si/AuNPs nanocomposites

The Si/AuNPs were prepared according to a published procedure with slight modification.[30] Briefly, alcohol (EtOH; 2600 μL), H_2O (500 μL), and ammonia-water ($NH_3 \cdot H_2O$; 300 μL) were mixed in a round-flask with stirring for 5 min. Tetraethyl orthosilicate (170 μL) was then added to the mixture and stirred for 8 h at room temperature. After the reaction, the mixture was centrifuged at 15,000 *g* for 10 min, rinsed successively with H_2O and EtOH three times, and then dried to obtain the silica particles.

The Au-coated silica complex was obtained by chemical reduction of an Au (III) solution with hydroxylamine in the presence of suspended silica nanoparticles. Firstly, SiO_2 (8 mg) was well dissolved in $HAuCl_4 \cdot 3H_2O$ (1 mL, 0.1 mg/mL), and then the solution was adjusted to pH 7-8 with 2 M NaOH, resulting in a colour change to pink. $NH_2OH \cdot HCl$ (30 μL, 0.22 M) was added for chemical

reduction of Au (III) to Au (0), and the colour immediately turned dark brown. The mixture was placed on an orbital shaker at 120 rpm for 10 h followed by resting for 10 h to discard the supernatant. The resulting nanocomplex was resuspended in H_2O. This procedure was repeated and the precipitated conjugates were dispersed in double-distilled water and stored at 4 °C.

Preparation of HRP-Si/AuNPs-Ab2 conjugates

First, the Si/AuNPs were sonicated with mercaptoacetic acid for 2 h to generate carboxylated groups, and then the mixture was washed repeatedly with PBS. Second, the carboxylated Si/AuNPs were added to 1.0 mL 400 mM EDC and 100 mM NHS in MES buffer (pH 5.2), and sonicated for 30 min. The mixture was centrifuged for 5 min at 13,000 *g* and the supernatant was discarded. Third, 500 µL of 400 ng/mL anti-CA153 and 500 µL of 80 µg/mL HRP were added to the mixture, which was stirred for 4 h at room temperature. The mixture was washed with PBS several times to remove unbound HRP and Ab2. Finally, the particles were dispersed in 1.0 mL of PBS (pH 7.4) containing 3% bovine serum albumin and stored at 4 °C.

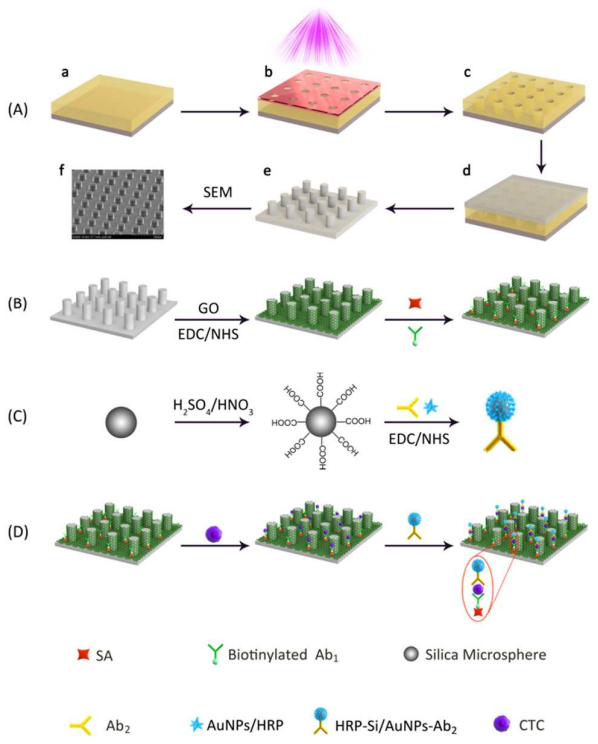

Scheme 1 (A) Schematic representation of the integrated fabrication of polydimethylsiloxane (PDMS)-based 3D microchip arrays. (B) The microchips were modified by GO, SA and biotinylated anti-EpCAM, respectively. (C) Si/AuNPs were synthesized and used as nanocarriers to load HPR and anti-CA153. (D) MCF7 cells bound to biotinylated anti-EpCAM and HRP-Si/AuNPs-Ab2 was recognized by MCF7 cells on the microchips.

Cell culture

MCF7 cells were cultured in DMEM supplemented with 10% fetal bovine serum, penicillin (100 µg/mL), and streptomycin (100 µg/mL) in an incubator (5% CO_2, 37 °C). After the concentration of cells reached 1 $\times 10^5$ cells mL^{-1}, the cells were collected using centrifugation at 1,000 *g* for 3 min.

Construction of the supersandwich cytosensor

The MCF7 cell suspension (100 µL) was introduced onto the modified 3D microchip device and kept in an incubator (5% CO_2, 37 °C) for 50 min, followed by washing with 0.05% Tween-20 and PBS. Then, 100 µL HRP-Si/AuNPs-Ab2 was dropped into the device and incubated at 37 °C for 50 min. After rinsing and staining, the immobilized cells were imaged by SEM and fluorescence microscope (Zeiss, Observer Z1), and analyzed with the CHI 660E electrochemical workstation. As a control, a flat substrate modified with GO/SA-Ab1 was also examined in parallel.

Results and Discussion

Characterization of Si/AuNPs and HRP-Si/AuNPs-Ab2 conjugates

The electrochemical responses were greatly influenced by the Ab2. So we first synthesized novel Si/AuNPs that were used as antibody and HRP carriers to amplify the signals. Figure 1A shows the SEM and transmission electron microscope images of the Si/AuNPs, indicating that the silica nanospheres were well covered with Au nanoparticles and the Si/AuNPs were mono-dispersed with a size around 125 nm in diameter. Such uniform dispersion of the Si/AuNPs was vital for their conjugation with HRP and Ab2. X-ray photoelectron spectroscopy (XPS) spectra were explored to confirm formation of the HRP-Si/AuNPs-Ab2 conjugate. As shown in Figure 1B, the conjugate exhibited some single sharp N, Si and Au peaks in the XPS spectra to indicate the successful formation of the HRP-Si/AuNPs-Ab2 conjugate.

Efficient capture of CTCs with the 3D microchip device

The 3D microstructure cell-capture device was prepared as illustrated in Scheme 1. To test the cell-capture performance of the 3D microchip device, we prepared a cell suspension (10^5 cells mL^{-1}) in cell culture medium (DMEM). The cell suspension (100 µL) was introduced onto the microchip device, which was placed in an incubator (5% CO_2, 37 °C) for 50 min. As controls, 3D microchip modified with SA-Ab1 and flat substrate modified with GO/SA-Ab1 were examined in parallel. After rinsing and staining, the substrate-immobilized cells were characterized through microscopy imaging and electrochemical behaviors. Figure 2A shows the SEM images of immobilized MCF7 cells at different magnifications after glutaraldehyde fixation. The immobilized MCF7 cells, which were stained with FDA, were also counted under a fluorescence microscope. As shown in figure 2B, the 3D microchips modified with

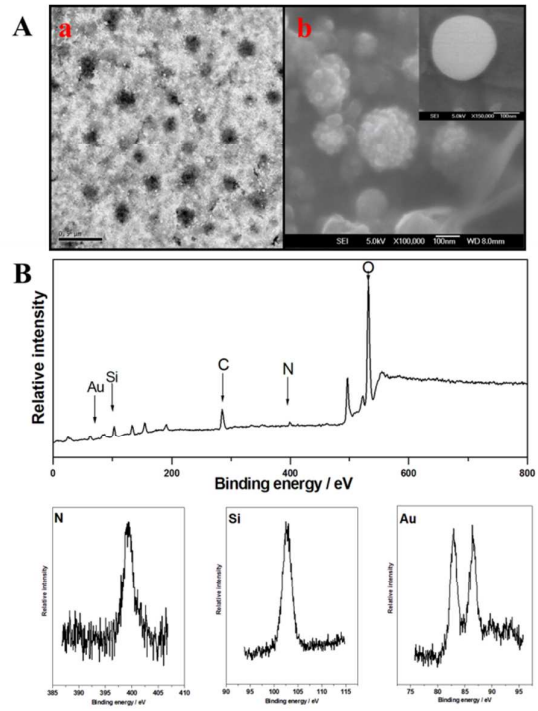

Figure 1 (A) TEM (a) and SEM (b) images of Si/AuNPs. Inset: SEM image of a silica nanosphere. (B) XPS spectra of HRP-Si/AuNPs-Ab2 conjugate.

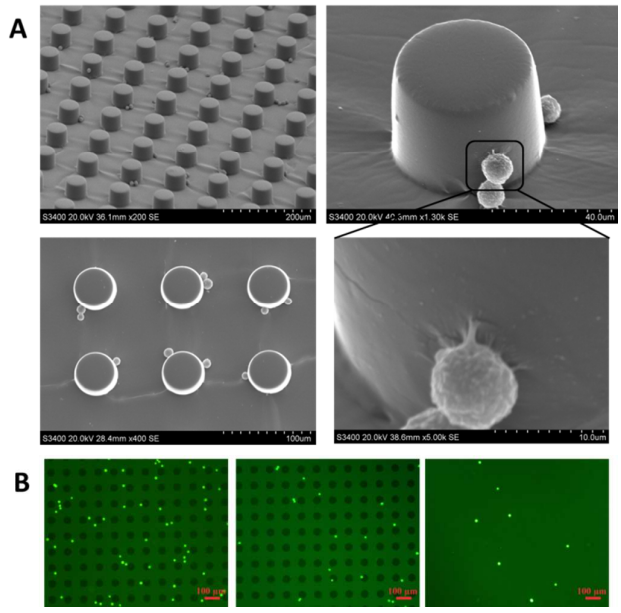

Figure 2 (A) SEM images of microchips on which MCF7 cells were captured, shown at different magnifications. (B) Fluorescence micrographs of 3D microchips modified with GO/SA-Ab1 (left), 3D microchips modified with SA-Ab1 (middle), and the flat substrate modified with GO/SA-Ab1 (right) on which MCF7 cells were captured.

GO/SA-Ab1 could capture three times more cells than the microchips only modified with SA-Ab1, and eight times more cells than the flat substrate modified with GO/SA-Ab1. This result suggests that the introduction of GO and the 3D microstructure was possible responsible for the enhanced cell-capture yields. This effect was likely due to the synergistic interplay between GO and the 3D microchip, which provided more surface area for SA and antibody binding and enhanced local topographic interactions between the microarrays and CTCs.

Characterization of the supersandwich cytosensor

As shown in Figure 3 (curve a), the cyclic voltammogram did not display any detectable signal on the Ab1-SA/GO/microchip in PBS (pH 7.4). However, upon addition of thionine and H_2O_2, a couple of stable and well-defined redox peaks were observed at -0.248 and -0.289 V (curve b), which corresponded to the electrochemical response of thionine. When the cytosensor was incubated with MCF7 cells at 10^5 cells mL^{-1}, no obvious change in the signal was observed (data not shown). However, after the sensor was incubated with the HRP-Ab2 solution, the reduction current obviously increased on the HRP-Ab2/MCF7/Ab1-SA/GO/microchip, which was due to the catalysis of the immobilized HRP toward the reduction of H_2O_2. Moreover, when replacing HRP-Ab2 with HRP-Si/AuNPs-Ab2 as the detection antibody, the electrocatalytic current at the HRP-Si/AuNPs-Ab2/MCF7/Ab1-SA/GO/microchip (curve d) increased substantially. As expected, the achieved amplification of the signal was ascribed to the increased amounts of enzymes introduced on the microchips compared with the traditionally labeled HRP-Ab2.

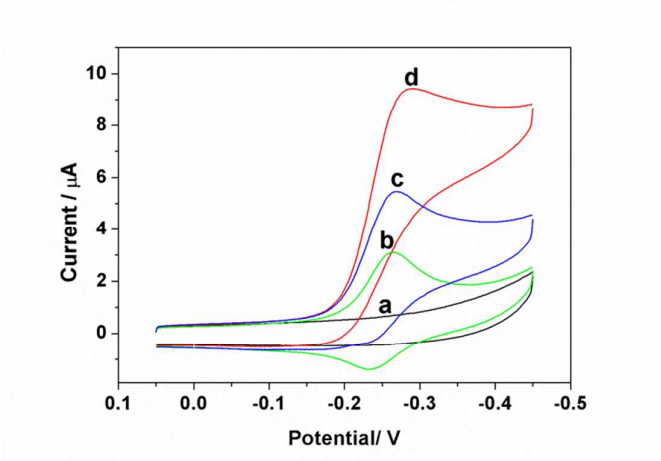

Figure 3 Cyclic voltammograms of (a) Ab1-SA/GO/microchip in pH 7.4 PBS and (b) Ab1-SA/GO/microchip, (c) HRP-Ab2/MCF7/Ab1-SA/GO/microchip, (d) HRP-Si/AuNPs-Ab2/MCF7/Ab1-SA/GO/microchip in pH 7.4 PBS containing 50 μM thionine and 2 mM H_2O_2. A concentration of 10^5 MCF7 cells mL^{-1} was used.

Optimization of experimental conditions

The electrochemical performance of the cytosensor is influenced by some parameters such as the ratio of HRP to Ab2 and the incubation time. To improve the sensitivity, the ratio of HRP to Ab2 was optimized first because of the co-immobilization of enzymes and antibodies on the Si/AuNPs nanocarrier. As shown in Figure 4A, a markedly increase of the peak current was observed when increasing the HRP/Ab2 ratio from 50/1 to 200/1. This increased ratio caused an increase total amount of HRP loaded per Si/AuNPs, which was expected to enhance the response during the immunoassay. However, the excessive HRP reduced the available binding sites of Si/AuNPs with Ab2, which would decrease the immune coupling efficiency for capturing MCF7 cells and result in a decreased response. Therefore, the HRP/Ab2 ratio of 200/1 was selected as the optimal condition for the preparation of HRP-Si/AuNPs-Ab2 conjugates. The BCA protein assay [31] showed that the concentration of active HRP in the HRP-Si/AuNPs-Ab2 dispersion was 4.31 μg mL^{-1}.

In addition, the effects of incubation time on the capturing MCF7 cells and the specifically recognizing HRP-Si/AuNPs-Ab2 were investigated. With increasing incubation time in the MCF7 solution, the peak current increased and tended to steady after 50 min (red curve in Fig. 4B), indicating thorough capturing of MCF7 cells on the 3D microchip device. When HRP-Si/AuNPs-Ab2 was incubated with MCF7 in the second step, the current increased and reached a plateau at 50 min (black curve in Fig. 4B), reflecting the saturated of binding sites between MCF7 and Ab2. Longer incubation time could result in a large nonspecific signal. Therefore, the optimal incubation time for the first and second immunoreactions was determined to be 50 min, respectively.

Electrochemical detection of CTCs

For the detection of CTCs, high sensitivity and selectivity play important roles in improving treatment. In view of this, the proposed supersandwich cytosensor was challenged with different concentrations of MCF7 cells, as shown in Figure 5A. The differential pulse voltammetry currents increased with increasing concentration of MCF7 cells. Figure 5B shows the linear calibration plots of the peak current (i_p) versus the concentration of MCF7 cells. A linear relationship between i_p and the logarithm of the cell concentration is found in the range of 10^1 - 10^7 cells mL^{-1}, with a correlation coefficient of 0.9921 (n = 3). The detection limit at a signal-to-noise ratio of 3σ (where σ is the standard deviation of the signal in a blank solution) was estimated to be 10 cells mL^{-1}, which is comparable and much lower than the values reported in the literature (summarized in Table 1). The excellent sensitivity is attributed to double signal amplifications from GO and Si/AuNPs, which greatly accelerate the rate of electron transfer on the cytosensor.

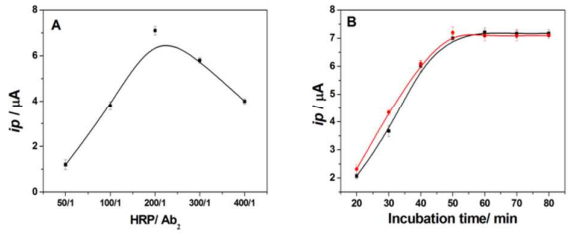

Figure 4 (A) Effects of the HRP to Ab2 ratio on the current responses in the presence of 10^5 MCF7 cells mL^{-1}. (B) Effect of incubation time on the current responses by capturing MCF7 (red curve) and recognizing between HRP-Si/AuNPs-Ab2 and MCF7 (black curve) in the presence of 10^5 MCF7 cells mL^{-1}.

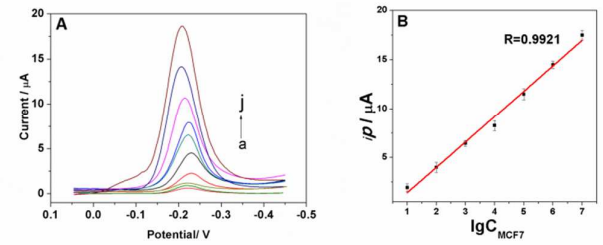

Figure 5 (A) Differential pulse voltammetry responses of the supersandwich cytosensor incubated with (b) Hela cells, (c) A549 cells at 10^5 cells mL^{-1} and (a, d-j) different concentrations of MCF7 cells: 0, 10^1, 10^2, 10^3, 10^4, 10^5, 10^6, 10^7 cells mL^{-1}. (B) Calibration curve of MCF7.

Table 1 Comparison of the sensitivity of different CTC cytosensors

Cytosensor type	Linear range (cells mL^{-1})	Detection limit (cells mL^{-1})	Reference
Microchip Cytosensor	10^1 to 10^7	10	Present study
LSAW Aptasensor	10^2 to 10^7	32	32
PEC Biosensor	10^2 to 10^6	58	33
Colorimetric Aptasensor	10^2 to 10^4	40	34
Aptamer/QDs Cytosensor	10^2 to 10^6	50	35

Performance of the supersandwich cytosensor

To investigate the specificity of the supersandwich cytosensor toward MCF7 cells, different possible interfering cells such as Hela and A549 were used. As shown in Fig. 5A (curves b and c), the peak current of the cytosensor showed a negligible change with the addition of the interfering cells, whereas a substantial

electrochemical signal increase was observed with the addition of MCF7 cells. These results demonstrated the good selectivity of the cytosensor for MCF7 cells. Thus, the proposed strategy can be applied to different types of CTCs using corresponding Ab2.

To evaluate the intra- and inter-assay coefficients of variation of the cytosensor array, the intra-assay precision of the proposed method was measured for six replicate measurements. The coefficients of variation of intra-assay were 3.5% at 10^5 cells mL^{-1}. Likewise, the inter-assay coefficients of variation on six cytosensor were 4.3% at 10^5 cells mL^{-1}. The precision and reproducibility of the cytosensor are acceptable. Moreover, when the cytosensor was stored at 4 °C, the analytical performance did not decline obviously after one week, and 93% of the initial response remained after one month. The stability is attributed to the stable structure of the Si/AuNPs and the strong interaction between anti-EpCAM and GO modified 3D microchips. Thus, the designed strategy shows good performance for the detection of CTCs with a broad detection range, low detection limit, excellent selectivity, good reproducibility and stability.

In this study, the supersandwich cytosensor shows attractive performance for the quantification of MCF7 cells, such as its wide linear range and low detection limit. First, the GO modified 3D microchips provide large specific surface areas to facilitate abundant binding of SA. Combined with the extraordinary biocompatibility of GO, the microchips are very suitable for immobilizing anti-EpCAM with excellent stability and bioactivity. Therefore, an ideal interface for cell capture is provided, which improves the sensitivity of detection compared to previous designs. Second, the supersandwich strategy helps to further enhance the sensitivity *via* the signal amplification of Si/AuNPs. Indeed, the introduction of an HRP-Si/AuNPs-Ab2 probe led to a remarkable increase of the signal.

Conclusions

In summary, since the local topographic interactions between the substrate and CTC increase, the sandwiches-like structure formed and double signal amplifications by using of GO and Si/AuNPs, the proposed supersandwich cytosensor shows excellent performance for analysis of CTCs with a wide linear range, low detection limit, and acceptable stability, reproducibility and accuracy. Among the various technologies developed to specifically recognize and capture CTCs to date, this is the first strategy to combine 3D microchips and an electrochemical method for quantitative detection of CTCs. Therefore, we anticipate that this 3D microchip device can be extended for the determination of other CTCs and show great potential in the field of disease diagnostics and clinical analysis.

Acknowledgements

This work was supported by National Natural Science Foundation of China (No. 81402466) and Natural Science Foundation of Hubei (No. 2015CFB610). W. Z. would like to acknowledge the support from a Jianghan University start-up grant. We would like to thank Editage (http://www.editage.cn/) for English language editing.

References

1 M. Cristofanilli, G. T. Budd, M. J. Ellis, A. Stopeck, J. Matera, M. C. Miller, J. M. Reuben, G. V. Doyle, W. J. Allard, L. W. M. M. Terstappen and D. F. Hayes, *N. Engl. J. Med.,* 2004, **351**, 781.
2 K. Pantel and C. Alix-Panabieres, *Trends Mol. Med.,* 2010, **16**, 398.
3 V. Murlidhar, M. Zeinali, S. Grabauskiene, M. Ghannad-Rezaie, M. S. Wicha, D. M. Simeone, N. Ramnath, R. M. Reddy and S. Nagrath, *Small,* 2014, **10**, 4895.
4 T. JunáHuang, *Lab chip,* 2013, **13**, 602.
5 S. Nagrath, L. V. Sequist, S. Maheswaran, D. W. Bell, D. Irimia, L. Ulkus, M. R. Smith, E. L. Kwak, S. Digumarthy, A. Muzikansky, P. Ryan, U. J. Balis, R. G. Tompkins, D. A. Haber and M. Toner, *Nature*, 2007, **450**, 1235.
6 S. K. Singh, C. Hawkins, I. D. Clarke, J. A. Squire, J. Bayani, T. Hide, R. M. Henkelman, M. D. Cusimano and P. B. Dirks, *Nature,* 2004, **432**, 396.
7 S. S. Banerjee, A. J. Badhwar, K. R. Zope, K. J. Todkar, R. R. Mascarenhas, G. P. Chate, G. V. Khutale, A. Bharde, M. Calderon and J. J. Khandare, *Nanoscale,* 2015, **7**, 8684.
8 X. Hu, C.W. Wei, J. Xia, I. Pelivanov, M. O'Donnell and X. Gao, *Small,* 2013, **9**, 2046.
9 A. K. Geim, *Science,* 2009, **324**, 1530.
10 G. S. Kulkarni, K. Reddy, Z. Zhong and X. Fan, *Nat. Commun.,* 2014, **5**, 4376.
11 R. Alam, I. V. Lightcap, C. J. Karwacki and P. V. Kamat, *ACS Nano,* 2014, **8**, 7272.
12 J. Wang and X. Qu, *Nanoscale,* 2013, **5**, 3589.
13 H. K. Choi, H. Y. Jeong, D. S. Lee, C. G. Choi and S. Y. Choi, *Carbon,* 2013, **14**, 186.
14 X. Zhang, Y. Zhang, Q. Liao, Y. Song and S. Ma, *Small,* 2013, **23**, 4045.
15 H. J. Yoon, T. H. Kim, Z. Zhang, E. Azizi, T. M. Pham, C. Paoletti, J. Lin, N. Ramnath, M. S. Wicha, D. F. Hayes, D. M. Simeone and S. Nagrath, *Nat. Nanotechnol.*, 2013, **8**, 735.
16 S. Yin, Y. L. Wu, B. Hu, Y. Wang, P. Cai, C. K. Tan, D. Qi, L. Zheng, W. R. Leow, N. S. Tan, S. Wang and X. Chen, *Adv. Mater. Interfaces*, 2014, **1**, 1300043.
17 H. J. Yoon, M. Kozminsky and S. Nagrath, *ACS Nano,* 2014, **8**, 1995.
18 N. Zhang, Y. Deng, Q. Tai, B. Cheng, L. Zhao, Q. Shen, R. He, L. Hong, W. Liu, S. Guo, K. Liu, H. R. Tseng, B. Xiong and X. Z. Zhao, *Adv. Mater.,* 2012, **24**, 2756.
19 S. Hou, L. Zhao, Q. Shen, J. Yu, C. Ng, X. Kong, D. Wu, M. Song, X. Shi, X. Xu, W. H. OuYang, R. He, X. Z. Zhao, T. Lee, F. C. Brunicardi, M. A. Garcia, A. Ribas, R. S. Lo and H. R. Tseng, *Angew. Chem. Int. Ed.,* 2013, **52**, 3379.
20 S. Hou, H. Zhao, L. Zhao, Q. Shen, K. S. Wei, D. Y. Suh, A. Nakao, M. A. Garcia, M. Song, T. Lee, B. Xiong, S. C. Luo, H. R. Tseng and H. H. Yu, *Adv. Mater.,* 2013, **25**, 1547.
21 S. Wang, K. Liu, J. Liu, Z. T. F. Yu, X. Xu, L. Zhao, T. Lee, E. K. Lee, J. Reiss, Y. K. Lee, L. W. K. Chung, J. Huang, M. Rettig, D. Seligson, K. N. Duraiswamy, C. K. F. Shen and H. R. Tseng, *Angew. Chem. Int. Ed. Engl.*, 2011, **50**, 3084.

22 X. Liu and S. Wang, *Chem. Soc. Rev.*, 2014, **43**, 2385.
23 O. Yehezkeli, R. Tel-Vered, S. Raichlin and I. Willner, *ACS Nano,* 2011, **5**, 2385.
24 Z. K. Han and Y. Gao, *Nanoscale,* 2015, **7**, 308.
25 A. Li, P. Zhang, X. Chang, W. Cai, T. Wang and J. Gong, *Small,* 2015, **11**, 1892.
26 W. Chen, P. H. Tsai, Y. Hung, S. Chiou and C. Y. Mou, *ACS Nano,* 2013, **7**, 8423.
27 D. Tarn, D. P. Ferris, J. C. Barnes, M. W. Ambrogio, J. F. Stoddart and F. I. Zink, *Nanoscale,* 2014, **6**, 3335.
28 N. Z. Knezevic and V. S. Y. Lin, *Nanoscale,* 2013, **5**, 1544.
29 L. Zhu, H. Wang, X. Shen, L. Chen, Y. Wang and H. Chen, *Small,* 2012, **8**, 1857.
30 K. Leopold, M. Foulkes and P. J. Worsfold, *Anal. Chem.,* 2009, **81**, 3421.
31 M. M´evel, G. Breuzard, J. J. Yaouanc, J. C. Cl´ement, P. Lehn, C. Pichon, P. A. Jaffr`es and P. Midoux, *Chem. Bio. Chem.,* 2008, **9**, 1462.
32 K. Chang, Y. Pi, W. Lu, F. Wang, F. Pan, F. Li, S. Jia, J. Shi, S. Deng and M. Chen, *Biosens. Bioelectro.,* 2014, **60**, 318.
33 F. Liu, Y. Zhang, J. Yu, S. Wang, S. Ge and X. Song, *Biosens. Bioelectro.,* 2014, **51**, 413.
34 X. Zhang, K. Xiao, L. Cheng, H. Chen, B. Liu, S. Zhang and J. Kong, *Anal. Chem.,* 2014, **86**, 5567.
35 H. Liu, S. Xu, Z. He, A. Deng and J. Zhu, *Anal. Chem.,* 2013, **85**, 3385.